Comparison of hydrogen retention in W and W/Ta alloys

K. Schmid *, V. Rieger, A. Manhard
Max-Planck-Institut für Plasmaphysik, EURATOM Association,
Boltzmannstraße 2, D-85748 Garching b. München Germany

Abstract

The extreme brittleness of tungsten (W) is one of the challenges of using W as first wall material. One attempt to alleviate this problem is to use W alloys with better mechanical properties. However these alloying elements must not degrade the favorable properties of W with respect to its application at the first wall of fusion devices: low sputter yield and hydrogen inventory.
In this work we investigate the hydrogen retention in the recently proposed W/Ta alloys under deuterium ion bombardment. By directly comparing pure W and W/Ta alloys with 1% and 5% Ta content we found that the W/Ta alloys retain significantly more hydrogen than pure W under identical implantation conditions.
Our finding of increased hydrogen retention together with the fact that the Ta alloying did not improve the brittleness makes W/Ta alloys an unacceptable choice for the first wall of fusion devices.

1 Introduction

The choice of the first wall material is one of the main challenges towards the realization of an energy producing fusion power plant. Materials facing plasmas in fusion experiments and future reactors are loaded with high fluxes (10^{20} to 10^{24} $m^{-2}s^{-1}$) of H, D, T fuel particles at energies between a few eV to keV. In this respect, the evolution of the radioactive T inventory in the first wall, the permeation of T through the armor into the coolant and the thermo-mechanical stability after long term exposure are key parameters determining the applicability of a first wall material [1].

*Corresponding Author
Tel: +49 89 3299 2228
Fax: +49 89 3299 2279
E-mail: Klaus.Schmid@ipp.mpg.de

Tungsten (W) is a candidate material for the first wall of fusion devices. It features a low vapor pressure and sputter yield, making it resilient against the interaction with fusion plasma. With respect to hydrogen retention, W features a very low solubility [2] and thus should retain very little hydrogen. But in reality the amount of retained hydrogen is governed by trapping at defects and not by the hydrogen dissolved in the lattice [3]. After plasma operation solute hydrogen will diffuse out and the remaining inventory will consist of hydrogen trapped in lattice defects, such as dislocations, grain boundaries, and irradiation induced traps [3].

Adding alloying components to W may provide additional binding sites for hydrogen and may thus increase the retention. In particular, the use of a hydride former like Ta may increase the retention in W. To investigate the influence of different Ta alloy concentrations in W on the hydrogen inventory, W samples with 1% and 5% Ta were compared to pure W sample exposed to deuterium (D) ions under identical implantation conditions. The total D inventory was investigated by thermal effusion spectroscopy (TES) [4] and the near surface depth profile by nuclear reaction analysis (NRA) [5]. Both NRA and TES show significantly higher retention of the implanted D in the W/Ta alloys compared to pure W. To understand the differences found between W and W/Ta alloys the depth profiles and TES spectra were modeled using a diffusion trapping model similar to model used in [6].

The paper will first present the sample preparation and characterization of the grain structure of the W and W/Ta samples used. Then the experimental conditions during implantation and the parameters of the TES and NRA measurements together with the results will be given. Next the model used to interpret the data will be described and the modeling results presented. Finally, the experimental and modeling results will be discussed.

2 Experiment

2.1 Sample preparation and characterization

Both the pure W and the W/Ta alloys used in this work were powder metallurgy samples, manufactured by Plansee^{TM}. W/Ta samples with two different levels of Ta (1 and 5 weight percent) were investigated. They were cut by wire etching to 12x12x0.8 mm^3. The residue from the wire cutting process was removed by coarse grinding of the sample with SiC sand paper. Then the samples were

polished to mirror finish with a final polishing step involving chemical etching to remove the distorted surface layer due to the previous mechanical polishing steps. After polishing and ultrasonic cleaning the samples were degassed in a high-vacuum furnace at a pressure of 10^-4 Pa and a temperature of 1200 K for 12 h. During this preparation step dissolved H and other impurities are removed without leading to any recrystallization or grain growth.
After sample preparation the homogeneity of Ta concentration in the W/Ta alloys and the grain structure were investigated by secondary electron microscopy (SEM) in a Philips XL30 ESEM. For both the 1% and the 5% alloy the lateral distribution of Ta is homogenous as determined from a 2D energy dispersive X-ray spectroscopy (EDX) map. The grain size was different for the pure W and the W/Ta alloys as can be seen in Fig. 1. The average grain size for the W/Ta alloy is $\approx 0.5\mu$m. For the pure W sample with $\approx 0.5 - 2\mu$m. So the grain size variation across the different sample types is still not too large.

2.2 Implantation

The implantations were performed in the high current ion source at IPP-Garching [7]. A beam of D_3^+ ions is extracted by 6 kV from an arc ignited in a Dua-Pigatron source. The beam is mass and energy separated in a 60° deflection magnet before it hits the sample. The typical beam currents that can be achieved for D ions is $\approx$ 20 to 50 μA. The corresponding ion beam flux Γ is typically in the order of 1×10^{19} D/(m^{2}s). The beam energy is determined by the 6 kV extraction voltage minus a 3 kV deceleration voltage at the target yielding 1keV/D implantation energy for a beam of D_3^+ ions. The target chamber is separated from the ion source by a differential pumping stage and has a base pressure of 10^{-7} Pa which increases to 10^{-5} Pa during ion beam operation.
All implantations were performed close to room temperature. The samples were heated by the ion beam to approximately 330K during the bombardment as measured by a thermocouple attached to the front (ion beam impact side) of the sample. During the implantation experiments the total ion fluence was varied by roughly one order of magnitude from 2×10^{23} to 1.2×10^{24} D/m^2. The above parameters represent a typical retention experiment and were performed many times (e.g. [4])on pure W thus making it a reasonable choice for the comparison of retention pure W with that in a W/Ta alloy.

3 Results

3.1 Nuclear reaction analysis

To determine the depth profile of D in W the ^{3}He(p, α)D nuclear reaction is used. The energy dependence of this nuclear reaction features a peak at $\approx$ 600 keV ^{3}He energy. Therefore varying the primary energy amounts to varying the depth being predominantly probed for D, since the ^{3}He ions lose energy as they penetrate the target [8]. Therefore for a given energy of the incident ^{3}He, the energy axis in the measured spectrum can also qualitatively be seen as a depth axis. The data measured at different ^{3}He energies need to be evaluated simultaneously to obtain the underlying depth profile. While this is done manually in [8] a more sophisticated automated program (NRADC) applying Bayesian statistics has been developed in [9]. In contrast to the manual method, this procedure produces an unbiased depth profile with statistically sound confidence intervals. The result of the data evaluation is a depth profile comprised of layers of a given width in units of areal density and height corresponding to the concentration of D in the layer. NRADC chooses the number of layers in the resulting depth profiles such that is minimizes the number of parameters required to describe the measured NRA data thus following Occam's razor principle [10].
In the experiments presented here the energy of the incident ^{3}He was varied from 600 keV to 4 MeV yielding a maximum information depth of $\approx$ 8 μm.
A comparison of the depth profiles determined by NRADC from the NRA data measured after implantation of pure W and W/Ta alloys are shown in Fig. 2. The depth profiles were measured after different D implantation fluences which also correspond to different implantation times. The x-scale of the depth profiles is given in μm which was calculated from the NRA depth scale in m^{-2} by dividing by the material number density which was assumed to be equal to that of bulk W (6×10^{28} m^{-3}). The most notable difference between pure W and the W/Ta alloys is that the alloys seem to have flatter profiles extending to larger depth as can be seen in Fig. 3. Also the alloy profiles show no decay but potentially even an increase towards larger depths. This is in strong contrast to the pure W which shows a decay towards larger depth. Already the depth profiles from the first $\approx$ 8 μm indicate that the W/Ta alloys retain more D than pure W.
The D concentration error bars given in the depth profiles are those that result form the statistical treatment of the data. They are very small due to the large

number of data points (in the order of several 10^3) compared to the small number of fit parameters i.e. concentrations (typically $\ll 10$). However the accuracy of the depth profiles depends also largely on the accuracy of the NRA spectra model used in the forward calculations performed in NRADC. Thus the error bars are only an estimate regarding the statistical significance of the data and are no absolute measure of the accuracy.

3.2 Thermal effusion spectroscopy

To determine the total amount of retained D the implanted samples were degassed in a TES setup. Apart from the total amount TES is also sensitive to the binding state (trapping) and the diffusion of D in the sample. To disentangle diffusion from trapping effects the thermally activated effusion process has to be modeled applying diffusion trapping codes (see section 4). From these models the binding (trap) energies can be estimated.
In the experiments presented here the TES measurement were performed in a chamber that is attached to the high current ion source and allows in vacuo transfer of the sample from the implantation chamber to the TES setup. In the TES chamber the sample is heated by an electron beam heater from the side opposite to the implanted side and its temperature is increased following an approximately linear ramp of ≈ 1 K/s from 300 K to 1200 K. The species effusing from the sample are detected by by a quadrupole mass spectrometer (Pfeiffer QMG700) whose ion source is facing the implanted side of the samples at a distance of ≈ 40 mm. The direct line of sight is blocked by a stainless steel plate, shielding the quadrupole from the electron gun acceleration voltage (3 kV) and the direct molecular beam. Thus the quadrupole measures only the contribution of the effusing species from the sample to the residual gas. This allows to quantitatively calibrate D_2, H_2 and HD signal in the quadrupole by comparing the current measured during the TES experiment with that corresponding to calibrated leaks. The calibration factor converting the measured ion current for a certain mass is given by the product of the ionization probability times the mass transmission through the quadrupole.
A D_2 and a H_2 leak, both with a leak rate of 2.45×10^{12} D_2 respectively H_2 per second were used to calibrate the quadrupole. These two leaks allow to calibrate the H_2 and D_2 signals. By assuming the same ionization rate coefficient for H_2, HD and D_2, a calibration factor for the HD signal (mass 3) can be interpolated by assuming a linear variation of the mass transmission between mass 2 (H_2)

and mass 4 (D_2).

Typical TES spectra for pure W and the W/Ta alloys with 1% and 5% Ta content are shown in Fig. 4. The pure W spectra appears quite different from the the W/Ta alloy spectra which all have the same qualitative shape, suggesting different binding states in the W/Ta alloys. However the broad nature of the peaks already suggests that the system is strongly influenced by diffusion. This makes it impossible to directly judge the trap site binding energies from the raw TES data. Therefore, detailed diffusion trapping modeling is required to understand the difference between pure W and W+Ta alloys.

What can be directly seem from the spectra in Fig. 4 is that the total retained amount is quite different: Pure W retains by far the least amount of D whereas 1% and 5% retain significantly more D.

Integrating the TES data vs measurement time (not vs temperature) yields the total amount of D retained in a sample. This assumes that all D is released up to the maximum temperature of ≈ 1200 K reached during the TES. The result of this total amount comparison is shown in Fig. 5 for pure W vs W + 5% Ta and W + 1% Ta. The total retention is given in units of D/m^2 which was calculated by dividing the total number of retained D obtained from TES by the area of the implantation spot which is $\approx 8 \times 6 \times 10^{-6}\ mm^2$. Again as was already indicated by the TES spectra in Fig. 4 and the NRA depth profiles in Fig. 2 the W+Ta alloys retain significantly more D that pure W. Also shown in Fig. 5 is the total amount within the NRA accessible range for W + 1% Ta. Except for the smallest fluence it is significantly lower than the TES result and it hardly varies with the implanted fluence. This suggests that the near surface area is quickly saturated and that most of the D is retained deep in the bulk.

While the NRA depth profiles were a bit different for W + 5% Ta and W + 1% Ta, the total amount from TES is essentially identical for both. This indicates that most retention occurs by decorating binding sites in the bulk, outside the range accessible to the NRA depth profile.

It is worth noticing that the actual dependence of retention is not one on fluence but on implantation time, i.e. the time the D has to diffuse into depth and populate the trap sites. So experiments done at vastly different fluxes can not be compared due to the different times required to reach a certain fluence.

4 Modeling

To model the implantation and retention of hydrogen species in metals typically diffusion trapping models are used [6, 11]. They are based on Fick's second law of diffusion with additional source (i.e implantation) and sink (i.e. trapping) terms as shown in eq. 1.

$$\frac{\partial C^{SOL}(x,t)}{\partial t} = D(T(t))\,\frac{\partial^2 C^{SOL}(x,t)}{\partial^2 x} + S(x,t) - \sum_{i=0}^{N^{Trap}-1} \frac{\partial C_i^T(x,t)}{\partial t} \tag{1}$$

$$\frac{\partial C_i^T(x,t)}{\partial t} = \frac{D(T(t))}{a_0^2\,\beta}\,C^{SOL}(x,t)\left(\eta_i(x,t) - C_i^T(x,t)\right) - C_i^T(x,t)\,\nu_i\,\exp\left(\frac{-E_i^{TS}}{k_B\,T(t)}\right)$$

$$S(x,t) = \frac{\Gamma}{\rho_0}\,\xi(x) \text{ with } \int_0^\infty \xi(x)\,dx \equiv 1$$

$C_i^T(x,t)$ = Concentration of hydrogen in trap type i

$C^{SOL}(x,t)$ = Concentration of solute hydrogen

$\eta_i(x,t)$ = Concentration of trap type i

$D(T(t))$ = Diffusion coefficient as function of temperature

$S(x,t)$ = Hydrogen source due to implantation with flux Γ $(m^{-2}s^{-1})$

$\xi(x)$ = Implantation range distribution $(1/m)$

ν_i, E_i^{TS} = Frequency factor (s^{-1}) and activation energy (eV) for detrapping from trap type i

ρ_0 = Density of target e.g. W

β = Number of solute sites per W atom

a_0 = Lattice constant of W

The Concentrations in the above equations are density fractions. The concentration of D is thus given as the density of D D/m^3 divided by the bulk number density ρ_0. Given the low D concentrations ρ_0 is essentially identical to number density of W, $6.2 \times 10^{28} m^{-3}$.
At the bombarded surface and at the opposite rear side of the sample different boundary conditions are possible. Hydrogen is released from an open surface into vacuum by recombining with another hydrogen atom at the surface and immediately desorbing as a D_2 molecule already at room temperature [4]. The process of recombination is usually not rate limiting for hydrogen desorption from

W [3, 4] and thus the complex recombination Neumann boundary condition can be replaced by a simple Drichlet boundary condition of C^{SOL} (0 or $\mathrm{x_{Max}}$, t) $\equiv 0$ (x_{Max} = Sample thickness). This boundary condition means that release from the surface is not limited by the surface process but by diffusion towards the surface.

To simultaneously fit both the depth profiles and the TES spectra required two different trap energies: 0.9eV and 1.2eV, $N^{Trap} = 2$ in Eq. 1. These numbers are in line with modeling results presented in [12].

The frequency pre-factors are of the order of 10^{13} s^{-1} but are often left as a fit parameter. The implantation source $S(x,t)$ is defined by the incident flux Γ and by the range distribution $\xi(x)$ which in the work presented here is approximated by a gaussian function with center R_P and width Δ_R, both obtained from a TRIM [13] calculation.

A key input into these models is the trap site distribution $\eta_i(x,t)$ for each trap i. Depending on the trap profile, multiple peaks in the TES spectra can appear, even for simulations with only a single trap site [14]. Since the trap profile is difficult to determine experimentally it introduces a large ambiguity into modeling TES data. One way to estimate the trap profiles is from NRA depth profiles measured at low (≈300K) temperatures. There all traps are decorated with D up to a depth limited by diffusion, thus the D depth profile is a representation of the total trap site concentration i.e. $\sum_{i=1}^{N^{Trap}} \eta_i(x,t)$. By comparing depth profiles measured at different implantation fluence (corresponding different implantation times) the advance of the diffusion front, filling the trap sites with D, can be observed. Potentially one can also observe the formation of new defects from the fluence dependence of the trap profile.

Following this procedure the trap site profiles can be estimated from the depth profiles in Figs. 2. For pure W a large difference exists between the depth profile at the lowest fluence to those measured after implantation at higher fluence. This suggests a time evolution of the trap site profile as was also found for implantation of pure W in [4]. Production of trap sites within the implantation range distribution is mostly due to kinetic energy effects. But additional trap sites can also be created outside the implantation zone through the stress field induced by the oversaturated implantation zone. This process saturates at high fluences as can be seen from the pure W NRA depth profiles in Figs. 2. The depth profiles measured at the higher fluences are essentially identical suggesting a saturation of the trap site formation.

In contrast to pure W the W + 5% Ta depth profiles are all essentially identical

suggesting that the trap production mechanism is overshadowed by the presence of intrinsic trap sites due to the Ta alloy atoms. Therefore a constant (i.e. fluence independent) trap site profile was assumed.
The NRA depth profiles only give a rough estimate of the total trap site distribution, for all trap types. To discern the trap site concentrations of different trap types one has to simultaneously fit both the depth profiles and the TES spectra, thereby maintaining the total local trap concentration.
A summary of the trap site concentrations and trap type parameters used in the simulations is shown in Fig. 6 for pure W and in Fig. 7 for W + 5%Ta. In Fig. 6 the evolving profile of trap type two and the constant profile of trap type one are shown together with frequency factors and de-trapping energies used in the simulations. In Fig. 7 the constant profile of trap type one and two are shown together with frequency factors and de-trapping energies used in the simulations. These assumptions may appear crude, but given the little information on the actual trap site distribution the aim was to model the data with as little parameters as possible to produce a simple model following the Occam's razor principle.
In addition to the trap profiles, the diffusion coefficient of the solute D must be given. As in most simulations dealing with D in W the values from Frauenfelder [2] are used. Since Frauenfelder's values were derived for hydrogen, the pre-exponential factor was scaled by $1/\sqrt{2}$ to account for the larger mass of deuterium.
We assume no annealing of defects during TES ramps up to 1200K which is supported by transmission electron imaging if pure W samples in [15]. There no change in the dislocation density is found up to 1200K. The combined fitting of depth profiles and TES spectra given the above input parameters is a two step process. In the first step the implantation of a certain fluence is simulated. This yields the depth profile of the retained D as solute and trapped at the different trap sites. In a second calculation step these profiles were used as initial conditions for a calculation of the TES spectra using the same parameters. In this calculation the source term in Eq. 1 was set to 0 and a time dependent sample temperature ramp $T^{Ramp}(t)$ is used. $T^{Ramp}(t)$ was thereby taken from the experimentally measured time evolution of the sample temperature during the individual TES measurements. Since the experimental temperature ramp has some noise it was replaced by a smooth polynomial fit to avoid stiffness problems during the numerical solution of Eq. 1.

5 Discussion

The retention of hydrogen species in W is commonly described as a diffusion limited filling of trap sites [3, 14]. These trap sites are either intrinsic or are produced by the incident species. The defect production can thereby either be kinetic displacement damage at high enough energies or by stress/strain produced by the over saturation within the implantation zone. We attribute the fluence evolution of the trap profile in pure W to the presence of stress fields due to over saturation of W. The existence of these stress fields can be based on the fact that blisters grow on W under D ion bombardment: To form blisters the material must be cracked by shear stress to allow for the formation of gas filled cavities. We believe that these shear stresses produce dislocations close (within the range of the NRA depth profile) to the surface which then act as trap sites for the D.

This basic mechanism explains the shape of the depth profiles in Figs. 2 and 3. Within the implantation range kinetic damage from the 1 keV/D and oversaturation by ion beam produce a large amount of trap sites resulting in the observed peak at the surface. Beyond the implantation range intrinsic and traps produced by the stress field resulting from the oversaturation at surface and are gradually filled in time by the moving front of diffusing D.

Comparing the depth profiles for pure W (dashed plots) with those for the W + 1%Ta alloy in Figs. 2 and 3 one finds that the alloy depth profiles obtained after similar implantation fluence/time are flatter and extend to greater depth. A comparison of the depth profiles of pure W with those of the W +5% Ta alloy in Fig. 2 also shows that the alloy has a flatter depth profile at similar implantation fluences/times. In addition the alloy depth profiles show the unexpected feature of an increase in the depth profiles at large depths. Initially this was thought be an artefact of the data evaluation but the NRA measurements were performed on different days together with the NRA measurements on pure W and on W + 1% Ta and only the W + 5% Ta samples showed this behavior. The increase was also visible in the raw data. Therefore we conclude that the data evaluation is correct and that the D concentration increases for large depths. Within the diffusion trapping picture the only explanation is that the intrinsic trap site density increases at larger depths for the W + 5% Ta alloy.

The total retained amount determined from TES is shown in Fig. 5. Again it becomes apparent that pure W retains less D than W+Ta alloys.

To understand the reason for the differences between W and W+Ta alloys diffu-

sion trapping modeling calculations were performed. As was already explained in section 4 the aim of the calculations was to find the trap site profile and de-trapping energies that best reproduce both the D depth profile and the TES spectra. The modeling calculations were limited to a comparison between W and W+5% Ta because there the differences were most apparent. Also to limit the calculation time only the lowest implanted fluence ($\approx 2 \times 10^{23}$ D/m^2) was modeled.

In Fig. 8 the calculated TES spectra of pure W and W + 5%Ta are compared. For this comparison the calibrated TES signal in units of D/s was converted to the units of effusion flux calculated by the model D/(μm^2 s) by dividing the TES signal by the beam spot area in μm^2. The match between the simulated and experimental data is very good both in terms of the qualitative shape and the quantitative amount of D released during TES. It should be pointed out that no normalization or scaling was applied, the model quantitatively simulates the experiment. The only difference between the input into the simulation for pure W and W+5%Ta was the trap site profile which was estimated from the NRA depth profiles in Fig. 2 as explained in section 4. The fact that the TES spectra look quite different shows the importance of the trap site profile in modeling TES spectra, a fact that's often neglected in modeling calculations.

As stressed before the model calculations were aimed at reproducing both the TES spectra and the depth profiles. In Fig. 9 a comparison of the D depth profiles after implantation that were used as initial conditions for the calculation of TES spectra in Fig. 8 are shown. The symbol graphs show the D depth profiles from NRA and the line only graphs show the calculated filling of the trap site profiles (see also Fig. 7). The correspondence between simulated and experimentally determined D depth profiles is still satisfactory, considering the rough estimate for the trap site profiles.

From good fit between model and experimental data one can conclude that the difference in retention between W and W+Ta alloys is due to additional intrinsic trap sites introduced by the Ta alloy component and not due to a higher diffusion coefficient.

Comparing the results obtained for W+1%Ta with those for W+5%Ta one finds that it lies close to, yet slightly below W+5%Ta with respect to retention. One may have expected a linear dependence of the total retention on the Ta concentration. However this is not to be expected since the retained amount does not just depend on the total amount of traps but also on whether or not they are reached by diffusion front. A larger trap concentration results in a reduced

effective diffusion coefficient since the trap sites hamper the penetration of the D depth profile. Therefore an increase in the trap site concentration does not result in an equal increase in the retained amount of D for implantations with the same flux and fluence. However the maximum potential retention is much higher since the total amount traps that can be filled given the time and fluence is much higher in the alloys that in pure W.

While the model in general results in a good reproduction of the measured data using the assumptions described in 4 there are still some inconsistencies related to the near surface peak ($\ll 0.5\mu m$). Looking closely at the pure W profiles in Fig. 2 one notices that, even within the large scatter of the NRA depth profile data, the surface peak is lower for fluences $> 2 \times 10^{23} m^{-2}$. This could be due to sputter removal of impurity induced trap sites at the surface.

Also comparing the surface peak of pure W and W+5%Ta one notices that the surface peak is not as pronounced in W+5%Ta which could be due to a different response of W+5%Ta to displacement damage (e.g. Formation of dislocations vs. formation of vacancy clusters).

Neither of these processes is currently taken into account in the model. The reason being that since retention is dominated by trapping in the bulk the ambiguities in modeling the surface peak do not affect the general conclusions drawn on the difference in retention in W vs. W/Ta alloys.

6 Conclusions

The retention of hydrogen in W and W/Ta alloys was compared. For all implantation conditions compared here the W/Ta alloys retain more D than pure W. By performing diffusion trapping model calculations it was possible to simulate both the measured NRA depth profiles and TES spectra. The modeling showed that both pure W and the alloys exhibit rather similar trap energies but the Ta in the alloys adds a large number of additional trap sites for hydrogen. This allows to conclude that the difference in retention between W and W/Ta alloys is due to a higher intrinsic trap density in the alloy due to the presence of Ta. This finding together with the fact that the Ta alloying did not improve [16, 17] the brittleness makes W/Ta alloys an unfavorable choice for the first wall of fusion devices.

Figure captions

Fig. 1
Grain structure of pure W a. and W/Ta with different Ta alloy concentration: b. 1%, c. 5%

Fig. 2
Comparison of depth profiles of pure W and W with 1% respectively 5% Ta for different implantation fluences.

Fig. 3
Direct comparison of depth profiles of pure W and W with 1% respectively 5% Ta at the lowest implanted fluence.

Fig. 4
Typical TES spectra obtained for a D fluence of $2 \times 10^{23} D/m^2$ for pure W and W/Ta alloys.

Fig. 5
Comparison of the total amount determined by TES for pure W, W + 5% Ta and W + 1% Ta. Also shown for comparison is the total amount within the first 8 μm from NRA for W + 1% Ta.

Fig. 6
Summary of the simulation parameters used in the model calculations for pure W. In particular the trap site profiles are shown for different fluences.

Fig. 7
Summary of the simulation parameters used in the model calculations for W +5%Ta. In particular the trap site profiles are shown.

Fig. 8
Comparison of experimental and calculated TES spectra for pure W and W + 5%Ta.

Fig. 9
Comparison of experimental and calculated D depth profiles for pure W and W + 5%Ta.

References

[1] J. Roth, E. Tsitrone, A. Loarte, T. Loarer, et al., J. Nucl. Mater. 390-391 (2009) 1.

[2] R. Frauenfelder, J. Vac. Sci. Technol. 6(3) (1969) 388.

[3] R. A. Causey, J. Nucl. Mater. 300 (2002) 91.

[4] O. V. Ogorodnikova, J. Roth, M. Mayer, J. Appl. Phys. 103 (2008) 034902.

[5] J. R. Tesmer, M. Nastasi, Handbook of Modern Ion Beam Materials Analysis, Material research society, Pittsburgh Pennsylvania, 1995.

[6] G. R. Longhurst, J. Ambrosek, Fusion Sci. and Tech. 48 (2005) 468.

[7] J. Roth, J. Bohdansky, W. Ottenberger, Technical report IPP 9/26, Max-Planck-Institut für Plasmaphysik, Boltzmannstrasse 2, 85748 Garching, Germany (1979).

[8] V. K. Alimov, M. Mayer, J. Roth, Nucl. Instrum. Meth. B 234 (2005) 169.

[9] K. Schmid, U. v. Toussaint, Statistically sound evaluation of trace element depth profiles by ion beam analysis, Nuclear Inst. Meth. B.

[10] D. S. Sivia, Data Analysis, A Bayesian Tutorial, Claredon Press, Oxford, 1996.

[11] A. H. M. Krom, A. Bakker, Metal. and Mat. Transact. B 31B (2000) 1475.

[12] M. Poon, A. Haasz, J. Davis, J. Nucl. Mater. 374 (2008) 390.

[13] W. Möller, W. E. und J. P. Biersack, Computer Physics Communications 51 No. 8 (1988) 355.

[14] T. J. Venhaus, R. A. Causey, Fusion Technology 39 (2) (2001) 868.

[15] A. Manhard, K. Schmid, M. Balden, W. Jacob, J. Nucl. Mater. 415 (2011) 632.

[16] D. Nguyen-Manh, M. Muzyk, K. Kurzydlowski, N. Baluc, M. Rieth, S. Dudarev, MATERIALS STRUCTURE & MICROMECHANICS OF FRACTURE 465 (2011) 15.

[17] M. Rieth, D. Armstrong, B. Dafferner, S. Heger, A. Hoffmann, et Al., Advances in Science and Technology 73 (2010) 11.

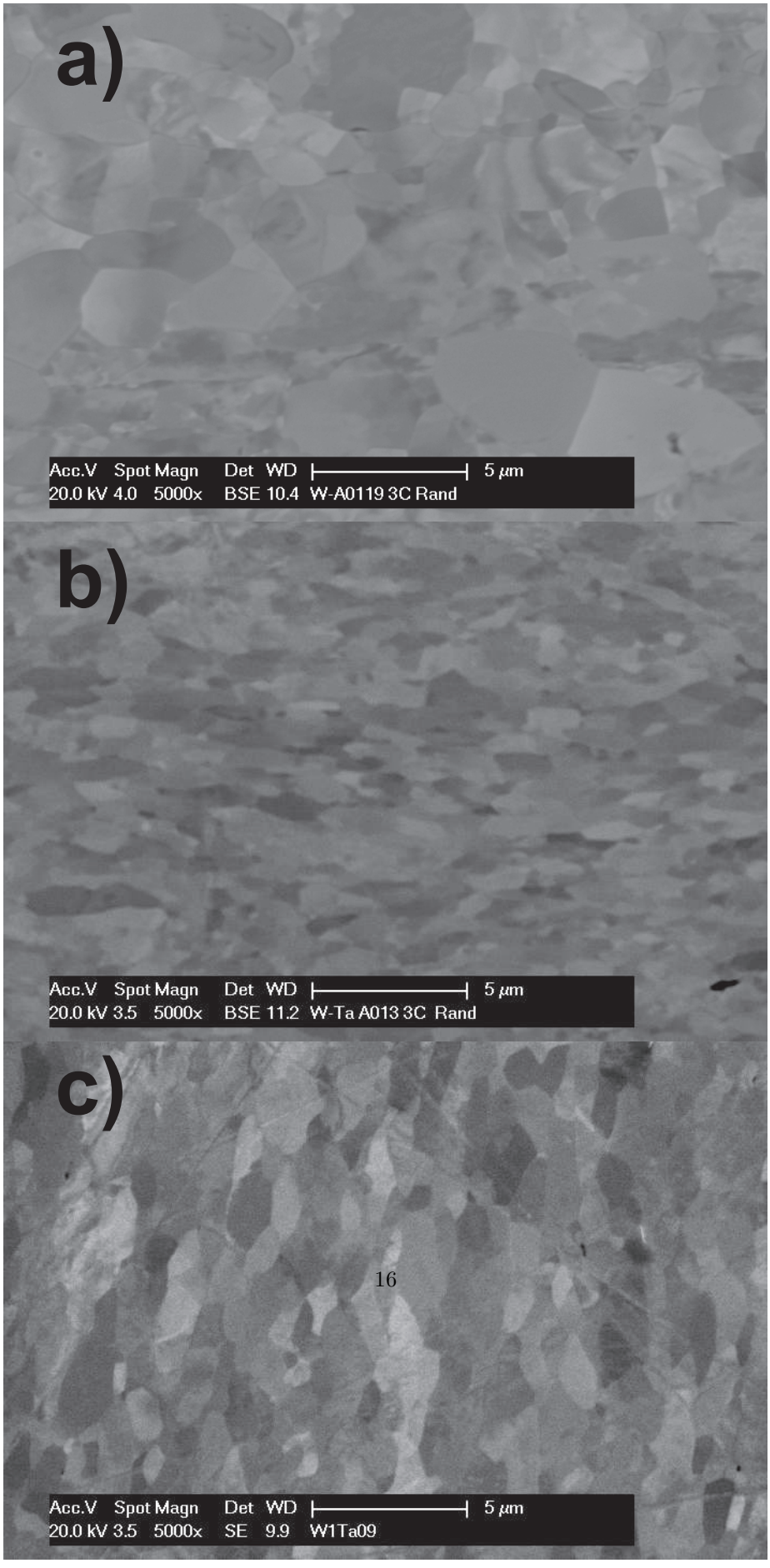
a)
Acc.V Spot Magn Det WD 5 μm
20.0 kV 4.0 5000x BSE 10.4 W-A0119 3C Rand
b)
Acc.V Spot Magn Det WD 5 μm
20.0 kV 3.5 5000x BSE 11.2 W-Ta A013 3C Rand
c)
Acc.V Spot Magn Det WD 5 μm
20.0 kV 3.5 5000x SE 9.9 W1Ta09

Figure 1

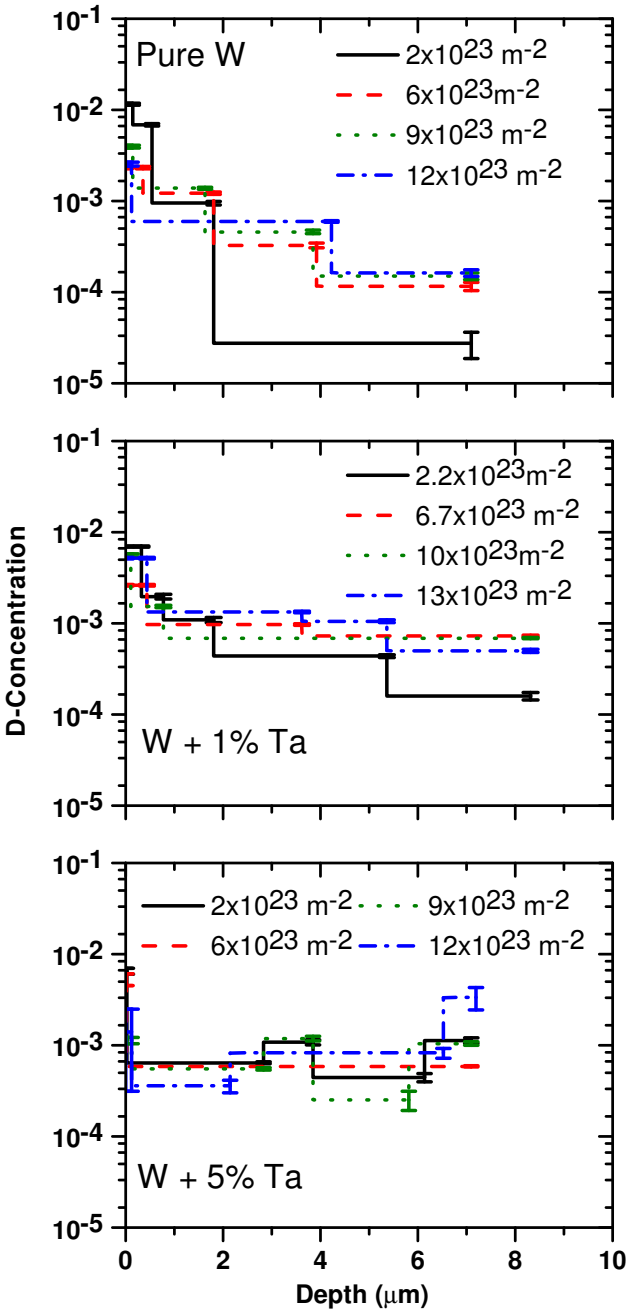
Pure W
2x10^23 m^-2
6x10^23m^-2
9x10^23 m^-2
12x10^23 m^-2
W + 1% Ta
2.2x10^23m^-2
6.7x10^23 m^-2
10x10^23m^-2
13x10^23 m^-2
W + 5% Ta
2x10^23 m^-2
6x10^23 m^-2
9x10^23 m^-2
12x10^23 m^-2
D-Concentration
Depth (μm)

Figure 2:

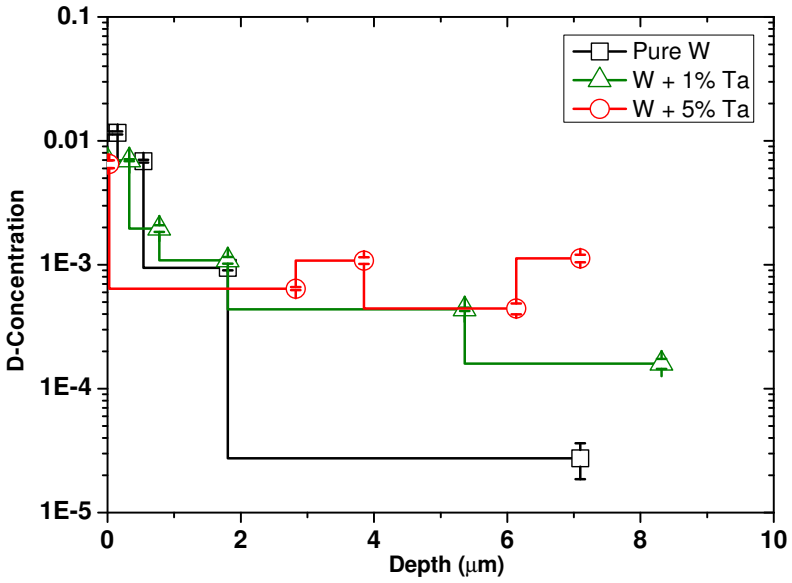
0.1
0.01
1E-3
1E-4
1E-5
D-Concentration
0
2
4
6
8
10
Depth (μm)
Pure W
W + 1% Ta
W + 5% Ta

Figure 3:

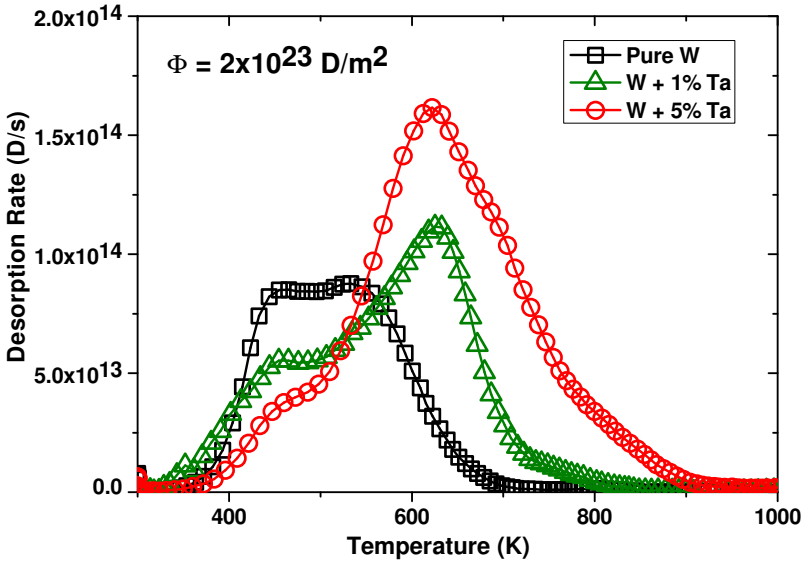
Φ = 2x10^23 D/m^2
Pure W
W + 1% Ta
W + 5% Ta
Desorption Rate (D/s)
2.0x10^14
1.5x10^14
1.0x10^14
5.0x10^13
0.0
400
600
800
1000
Temperature (K)

Figure 4:

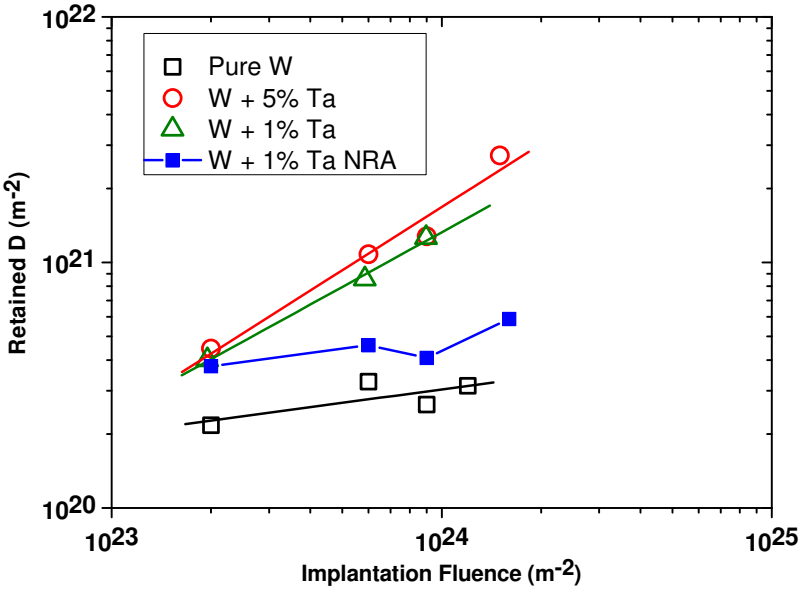
Pure W
W + 5% Ta
W + 1% Ta
W + 1% Ta NRA
Retained D (m-2)
Implantation Fluence (m-2)
10^22
10^21
10^20
10^23
10^24
10^25

Figure 5:

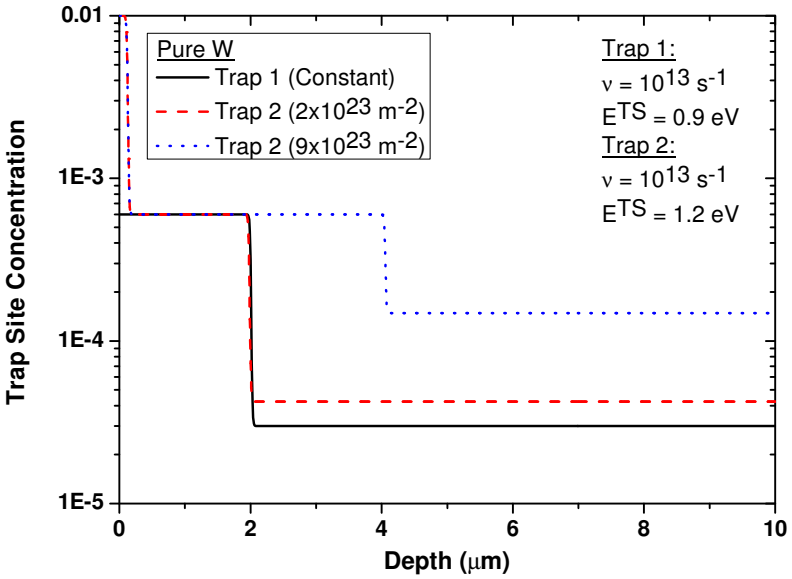
Pure W
Trap 1 (Constant)
Trap 2 (2x10^23 m^-2)
Trap 2 (9x10^23 m^-2)
Trap 1:
ν = 10^13 s^-1
E^TS = 0.9 eV
Trap 2:
ν = 10^13 s^-1
E^TS = 1.2 eV
Trap Site Concentration
0.01
1E-3
1E-4
1E-5
0
2
4
6
8
10
Depth (μm)

Figure 6:

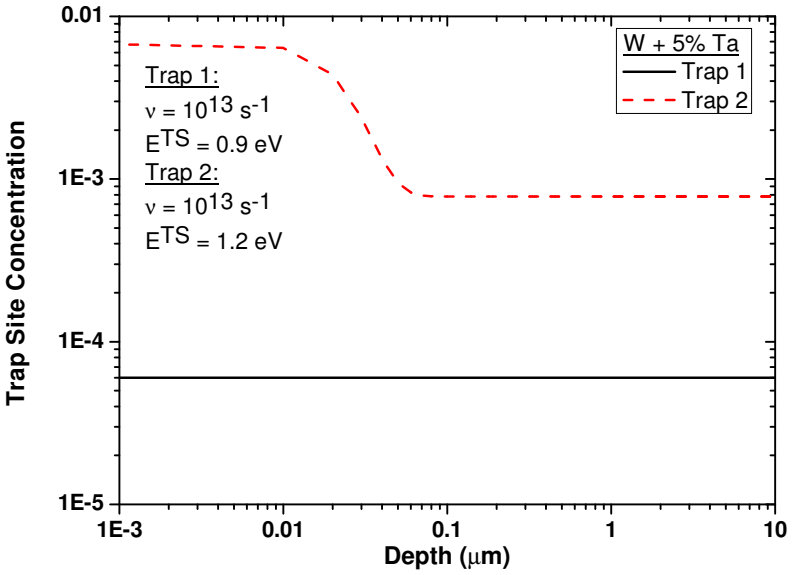
0.01
1E-3
1E-4
1E-5
Trap Site Concentration
1E-3
0.01
0.1
1
10
Depth (μm)
W + 5% Ta
Trap 1
Trap 2
Trap 1:
ν = 10^13 s^-1
E^TS = 0.9 eV
Trap 2:
ν = 10^13 s^-1
E^TS = 1.2 eV

Figure 7:

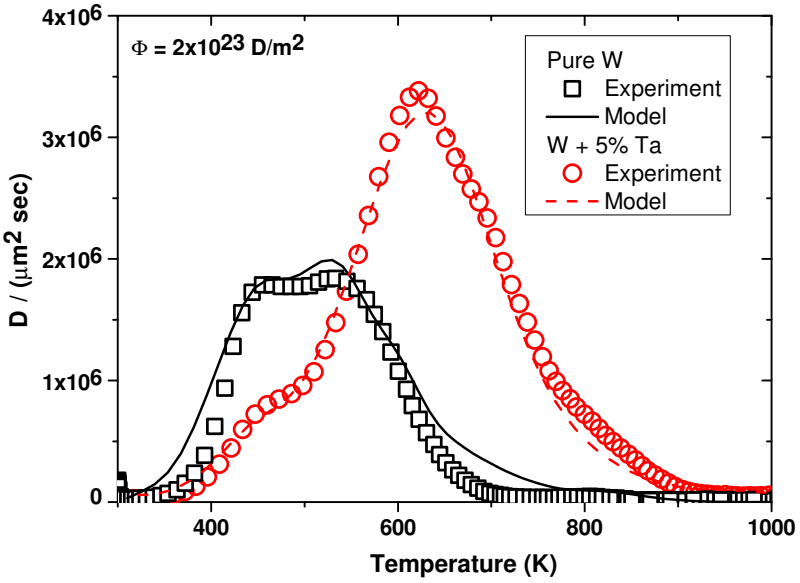
4x10^6
3x10^6
2x10^6
1x10^6
0
Φ = 2x10^23 D/m^2
Pure W
Experiment
Model
W + 5% Ta
Experiment
Model
D / (μm^2 sec)
400
600
800
1000
Temperature (K)

Figure 8:

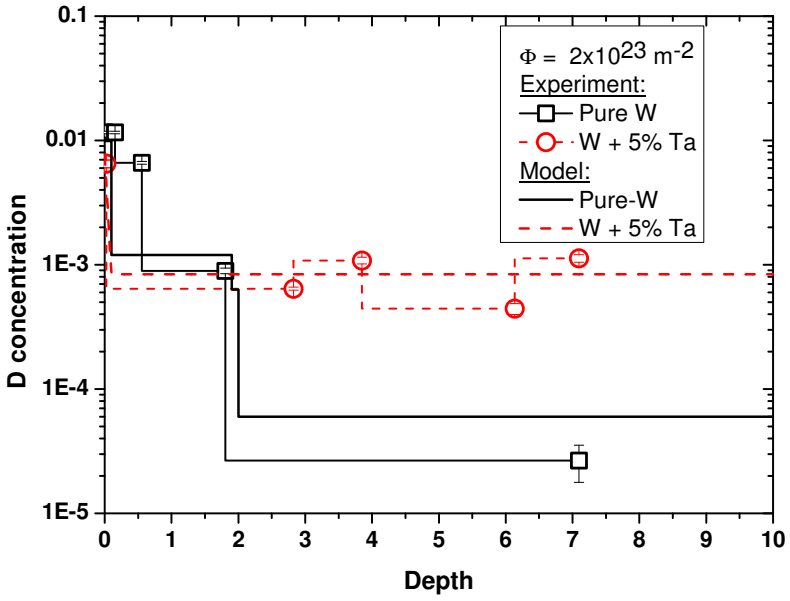
0.1
0.01
1E-3
1E-4
1E-5
D concentration
0
1
2
3
4
5
6
7
8
9
10
Depth
Φ = 2x10^23 m^-2
Experiment:
Pure W
W + 5% Ta
Model:
Pure-W
W + 5% Ta

Figure 9: